JOURNAL of the MEXICAN CHEMICAL SOCIETY

https://www.jmcs.org.mx/

Article

Open Access

*J. Mex. Chem. Soc.* **2026**, *70(1):e2561*

Received September 24th, 2025
Accepted March 3rd, 2026

http://dx.doi.org/10.29356/jmcs.v70i1.2561
e-location ID: 2561

**Keywords:**
$ZrCl_3$, supercell, adsorption system, dynamic simulation

**Palabras clave:** $ZrCl_3$; supercelda; sistema de adsorción; simulación de dinámica molecular

***Corresponding author:**
Doaa S. El Sayed
email: doaa.saeed@alexu.edu.eg, doaasaied75@yahoo.com



ISSN-e 2594-0317

# Structural Modification and $CO_2$-Adsorption Application on Unit Cell and Supercell Zirconium Chloride: Electronic, Dynamic and Hydrated Adsorption System

Dehbi Atallah[1], Ali Abdullah Issa[2], Doaa S. El Sayed[*3]

[1]Institute of Sciences, Nour Bachir University Center, El-Bayadh 32000, Algeria.
[2]College of Applied Science, University of Technology, Baghdad, Iraq.
[3]Chemistry Department, Faculty of Science, Alexandria University, Baghdad Street, Moharam Bey, P.O. Box 21511, Alexandria, Egypt.

**Abstract.** Structural modification of catalyzed materials for $CO_2$ adsorption involves altering their physical and chemical properties to enhance their capacity and efficiency in capturing carbon dioxide. $ZrCl_3$ crystal was considered to investigate its properties and modified aspects in the presence of $CO_2$ on the surface of the unit cell structure and the generated supercell. Frontier molecular orbitals (FMOs) of the designed systems were evaluated for the best describing the electronic variation in the presence and absence of $CO_2$ molecules. The presence of $CO_2$ molecule led to adsorption modification slightly changing the band gap with variation in orbital contribution on the surface of the catalyst. Molecular electrostatic potential (MEP) of the optimized structures was generated to give an insight into the most electrophilic and nucleophilic centers present before, and after $CO_2$ adsorption. The band gap calculated for the overall solid-state crystal at the same level of optimization was 2.35 eV expecting the semiconducting behavior. Molecular dynamic simulation over 10000 ps (10 ns) was considered and the results concluded a more stable $CO_2$-unit cell adsorption system with high capacity



*J. Mex. Chem. Soc.* **2026**, *70(1):e2561*
Regular Issue

ISSN-e 2594-0317

of adsorbate on the surface. A hydrated system adsorption locator was performed, where the adsorbate distribute itself freely inside the hydration layer. This indicates higher interaction with $H_2O$ molecules with significant adsorption energy ranges from -2.00 eV to -1.93 eV.

**Resumen.** La modificación estructural de materiales catalíticos para la adsorción de $CO_2$ consiste en alterar sus propiedades físicas y químicas con el fin de mejorar su capacidad y eficiencia para capturar dióxido de carbono. En este trabajo se estudió el cristal de $ZrCl_3$ para investigar sus propiedades y las modificaciones inducidas por la presencia de $CO_2$ sobre la superficie de la estructura de la celda unitaria y de la supercelda generada. Se evaluaron los orbitales moleculares de frontera (FMO) de los sistemas diseñados con el propósito de describir las variaciones electrónicas en presencia y ausencia de moléculas de $CO_2$. La presencia de $CO_2$ produjo modificaciones en la adsorción que ocasionaron ligeros cambios en la brecha de energía (band gap), acompañados de variaciones en la contribución de los orbitales sobre la superficie del catalizador. Asimismo, se calculó el potencial electrostático molecular (MEP) de las estructuras optimizadas para identificar los centros más electrófilos y nucleófilos antes y después de la adsorción de $CO_2$. La brecha de energía calculada para el cristal en estado sólido, al mismo nivel de optimización, fue de 2.35 eV, lo que sugiere un comportamiento semiconductor. Se realizaron simulaciones de dinámica molecular durante 10000 ps (10 ns), cuyos resultados mostraron que el sistema de adsorción $CO_2$–celda unitaria es el más estable y presenta una elevada capacidad para retener el adsorbato sobre la superficie. Además, se llevó a cabo un estudio de localización de la adsorción en un sistema hidratado, en el que el adsorbato se distribuye libremente dentro de la capa de hidratación. Este comportamiento indica una mayor interacción con las moléculas de $H_2O$, con energías de adsorción comprendidas entre −2.00 eV y −1.93 eV.

## Introduction

Various types of catalysts have unique properties and applications, making them essential in fields ranging from petrochemicals to pharmaceuticals and environmental science [1-3]. These materials offer significant research potential and have broad applications in solving diverse challenges. For example, perovskite materials have recently gained prominence in solar cell technology [4]. They exhibit excellent light-harvesting abilities, remarkable quantum efficiency, high charge carrier mobility, and tunable emission wavelengths. They also exhibit outstanding photoelectric conversion efficiency [5-7]. Conventional techniques for creating novel materials typically involve a lot of labor and resources along with a lot of trial and error. As science and technology have advanced, it has been found that computer simulations may be used to perform material computations [8-11]. First-principles techniques are widely employed in material calculation because they produce accurate and efficient computation results and have a solid theoretical foundation [12,13]. Numerous studies have revealed a strong agreement between the material properties computed from first-principal calculations and those derived from experimental synthesis, highlighting the usefulness of this approach for material experimentation. Strongly correlated gas adsorption materials with the different types of catalysts have generated a lot of interest in recent years for both experimental and theoretical studies [14-17]. Zr-catalyst materials can demonstrate novel characteristics in terms of electronics and magnetism, including superconductivity, enormous magnetoresistance, and semiconducting behavior [18]. As a result, they have a wide range of possible technological uses, such as optical resonators, magnetic storage devices, and storage device filters [19,20]. Zirconium-based double perovskites have garnered a lot of interest because of their possible uses in optical and electrical devices [21-23]. By forecasting how modifications to composition or structure will impact performance, computational methods can aid in the design of novel materials with desired qualities [24,25]. First-principles methods based on DFT provide a reliable framework for investigating adsorption energetics, charge transfer, and electronic structure modifications induced by adsorbate–substrate interactions. Numerous studies have demonstrated close agreement between DFT predictions and experimental observations for gas adsorption on metal halides, oxides, and low-dimensional materials, highlighting the suitability of these approaches for probing adsorption mechanisms prior to experimental realization. In particular, DFT enables the decomposition of adsorption behavior into contributions from geometry

http://dx.doi.org/10.29356/jmcs.v70i1.2561

*J. Mex. Chem. Soc.* **2026**, *70(1):e2561*
Regular Issue

ISSN-e 2594-0317

optimization, electronic redistribution, and orbital interactions, which is essential for physically meaningful interpretation.

Zirconium-based materials are of interest due to their chemical stability, strong affinity toward small molecules, and tunable coordination environments. While zirconium oxides and metal–organic frameworks have been extensively studied for gas capture, zirconium halides—such as $ZrCl_3$, remain comparatively less explored, despite their distinctive electronic structures and potential for surface reactivity. The layered or cluster-like nature of $ZrCl_3$ provides diverse adsorption sites whose interaction with $CO_2$ may vary significantly depending on dimensionality, coordination environment, and surface exposure.

Through the design, discovery, and optimization of innovative materials for a range of applications, from energy storage to structural components, computational research is transforming the field of materials science [26-28]. An alternative approach involves sampling a suitable physical distribution, specifically that of the canonical ensemble, through techniques such as the Metropolis algorithm or configurational bias method [29]. This process is implemented using the Sorption module, which analyzes the dynamic behavior of microscopic molecules within a matrix, along with the Amorphous Cell tool that generates periodic simulation cells. Finally, some more modules optimize a function by using simulated annealing and related methods. These modules estimate crystal structure from molecular structure. Polymorph Predictor, Powder Solve, and Adsorption Locator are among them.

In this work, we present a systematic first-principles investigation of $CO_2$ adsorption on $ZrCl_3$-based systems with increasing structural complexity. Isolated $ZrCl_3$ clusters, extended crystal planes, and multilayer supercell models are examined to clarify how structural dimensionality influences adsorption strength, electronic structure, and charge redistribution. Adsorption energies, optimized geometries, density of states, and related electronic descriptors are analyzed to establish physically consistent trends in $CO_2$ binding behavior. Particular attention is given to distinguishing physisorption from chemisorption characteristics based on energetic, geometric, and electronic criteria. The primary objective of this study is to provide a coherent and physically grounded description of $CO_2$ adsorption on $ZrCl_3$ materials using DFT-based methods. By correlating adsorption energetics with electronic structure modifications across different $ZrCl_3$ configurations, this work aims to clarify the underlying adsorption mechanism and assess the suitability of $ZrCl_3$-based systems for $CO_2$ capture applications. The insights gained from this analysis may serve as a reference for future theoretical and experimental investigations of metal halide–based adsorption materials.

## Computational methodology

All calculations were carried out using the Materials Studio software package [30]. The bulk $ZrCl_3$ crystal structure was first fully optimized within DFT using the Cambridge Sequential Total Energy Package (CASTEP) code [31–33]. The exchange-correlation contribution to the total energy was computed with the Perdew-Burke-Ernzerhof (PBE) generalized gradient density functional approximation (GGA) [34,35]. The interaction between valence electrons and ionic cores was described using on-the-fly generated (OTFG) ultrasoft pseudopotentials [36–38], and the electronic wavefunctions were expanded in a plane-wave basis set with a cutoff energy of 489 eV, which was verified to ensure total-energy convergence. Brillouin-zone integrations were performed using a Monkhorst–Pack k-point grid of 2 × 2 × 2 for bulk geometry optimization and total-energy calculations. Geometry optimizations were considered converged when the total energy change was less than $2 \times 10^{-5}$ eV/atom, the maximum force on each atom was below 0.05 eV $Å^{-1}$, the maximum stress was below 0.05 GPa, and the maximum atomic displacement was about $2 \times 10^{-3}$ Å.

To investigate surface–adsorbate interactions, a slab model was constructed by cleaving the optimized bulk structure along the (0 0 1) crystallographic plane, which corresponds to a low-index and energetically stable surface. The slab consisted of multiple atomic layers (2x2) with a vacuum thickness of 10 Å. During slab relaxation, the bottom layers were fixed at their bulk positions, while the upper layers were allowed to relax, simulating a semi-infinite surface. A supercell expansion was employed to minimize lateral interactions between adsorbed $CO_2$ molecules. The (0 0 1) surface was selected due to its structural stability and representative exposure of surface Zr sites, which are expected to dominate $CO_2$ adsorption behavior. Band structure and density of states (DOS) calculations were performed using the optimized slab geometry with the

http://dx.doi.org/10.29356/jmcs.v70i1.2561

*J. Mex. Chem. Soc.* **2026**, *70(1):e2561*
Regular Issue

ISSN-e 2594-0317

same *k*-point sampling to ensure consistency across electronic analyses. Because conventional GGA functionals do not adequately describe long-range dispersion forces, the Tkatchenko–Scheffler (TS) DFT+D correction [39] was included to account for van der Waals interactions, which are particularly important for weakly bound $CO_2$ adsorption. This correction allows for a more realistic description of adsorption energies and equilibrium geometries. A clear distinction is maintained between first-principles DFT calculations and classical molecular dynamics (MD) simulations. The DFT calculations were employed to analyze electronic structure, adsorption energies, and charge redistribution, while classical simulations were used to investigate the thermal stability and dynamic behavior of adsorbed $CO_2$ molecules. Classical molecular dynamics simulations were carried out using the Forcite module [40] with the COMPASS force field, which is well-suited for describing inorganic–organic interfacial interactions. MD simulations were performed in the canonical (NVT) ensemble at constant temperature, controlled using a thermostat, over a simulation time of 10 ns (10000 ps). This timescale was selected to ensure sufficient sampling of adsorption configurations and surface diffusion behavior. Finally, the Adsorption Locator module was employed to predict energetically favorable adsorption sites and orientations of $CO_2$ on the $ZrCl_3$ surface.

The adsorption energies reported for the hydrated systems correspond to total adsorption energies defined with respect to fully relaxed reference states of the isolated components. Specifically, the adsorption energy was calculated as [41]

$$E_{ads}=E_{ZrCl3+CO2+H2O}-(E_{ZrCl3+H2O}+E_{CO2}) \quad (1)$$

where $E_{ZrCl3+CO2+H2O}$ is the energy of the whole studied system, $E_{ZrCl3+H2O}$ is the energy of the hydrated $ZrCl_3$ layer, and $E_{CO2}$ is the energy of an isolated $CO_2$ molecule in vacuum. This definition ensures that the reported adsorption energies quantify the incremental stabilization arising from $CO_2$ uptake under hydrated conditions, rather than conflating hydration and adsorption effects.

To ensure accurate evaluation of adsorption energies, the potential influence of basis set superposition error (BSSE) was considered. In cluster-based calculations, BSSE arises from the artificial stabilization of the adsorbate due to the overlap of basis functions from the surface and the $CO_2$ molecule. To correct for this effect, counterpoise calculations were performed for representative adsorption configurations, following the Boys and Bernardi scheme [42].

$$E_{ads}^{BSSE}=E_{ZrCl3+CO2+H2O}-(E_{ZrCl3+H2O}+E_{CO2}) - \delta^{BSSE} \quad (2)$$

The adsorption energy corrected for basis set superposition error (BSSE), referred to as was calculated by including the $\delta^{BSSE}$ term. This correction employed the counterpoise (CP) method to reduce the artificial overestimation of interaction energy introduced by BSSE [43].

The most stable configurations obtained from Adsorption Locator were subsequently refined and validated through DFT geometry optimization and electronic-structure analysis, ensuring consistency between classical predictions and first-principles results.

## Results and discussion

### Carbon dioxide adsorption and electronic analysis of zirconium chloride system

Determining the type of surface interaction that occurs between an adsorbent and an adsorbate is required to understand the adsorption mechanism [44,45]. The geometrical shapes of the designed $ZrCl_3$ unit cell and supercell are displayed in Fig.1. The CASTEP primitive lattice with *k*-points for the first Brillouin zone of high symmetry was selected for optimum electronic analysis. The unit cell exported two Zr atoms with six Cl atoms to balance the charge of the cell. The supercell structure acts as a suitable surface for the adsorption process, where its Zr-Cl bonds are equal in length (2.56Å).

*J. Mex. Chem. Soc.* **2026**, *70(1):e2561*
Regular Issue

ISSN-e 2594-0317

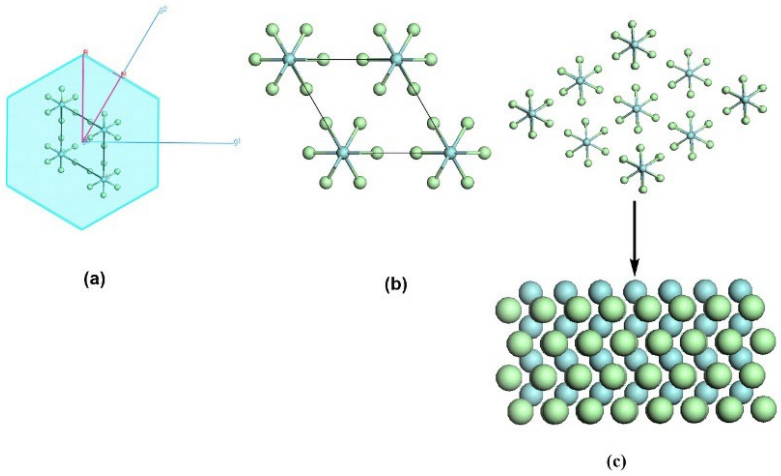


**Fig. 1. (a)** Reciprocal lattice structure of $ZrCl_3$ crystal in boundary conditions utilizing CASTEP, **(b)** $ZrCl_3$-optimized structure in unit cell and supercell generation, **(c)** atomic structure of 2X2 $ZrCl_3$- supercell (2x2) (atomic ball and stick in the upper panel and CPK style in the bottom of the panel).

The most accurate description for the combined molecular orbitals, and electronic distribution was found using FMO analysis of the optimized structural system [46]. Using energy level values, Fig. 2 shows the highest occupied (HOMO) and lowest unoccupied (LUMO) molecular orbitals that referred, in solid state, to valence band maximum and conduction band minimum, respectively. It was thought that the $ZrCl_3$ unit cell would have a chemically reactive structure before and after adsorption, since it has a little higher band gap (ΔE) with values of 2.28 eV for the pristine system and 2.34 eV after adsorption. This adsorption modification slightly raises ΔE with variation in orbital contribution on the surface of the catalyst. As shown in Fig. 2B, the $CO_2$-$ZrCl_3$ unit cell exhibited some rearrangement in the orbital contribution to face the $CO_2$ molecule. This predicts variation in electron transition for $ZrCl_3$ in an excited state. In the $ZrCl_3$ supercell, the pristine system gives an insight into its higher reactivity compared with the unit cell system due to the extra additive energy levels with increasing system size. Its valence band energy was counted by -4.54 eV compared with the $ZrCl_3$ unit cell (-6.31 eV), this notifies the active supercell surface with ΔE equal to 1.46 eV compared with the unit cell. Supercell with several $CO_2$ molecules adsorption system estimated its ΔE value with 1.40 eV, slightly less than of the pristine system. The orbital contribution on Zr and Cl atoms is attempted to be closer to the $CO_2$ molecules on the surface, predicting electronic excitation and interaction on the modified surface, especially oxygen contents occur in $CO_2$ molecules that may make some variation in $ZrCl_3$ electronic system.

The electronic density of the adsorbed system differs from that of the individual structures, as seen by the molecular electrostatic potential map, or MEP [47]. The red-colored patches in Fig. 3's MEP map for the color code "electron-rich sites" are largely found in the non-absorbed supercell system. While there are some balanced charge densities on the unit cell Zr-system before $CO_2$ adsorption. The yellow areas refer to some sites rich in electrons in which the electrostatic potential is low. However, $CO_2$ adsorption makes some changes to the surface based on its position. The system exported blue surface areas (electron deficiency sites). The study discovered that electron removal by $CO_2$ molecules and subsequent interaction resulted in some electron-poor areas on the Zr surface. The electron density variation is more obvious in the supercell system before and after adsorption, confirming the presence of $CO_2$ molecules as an electron acceptor, leading to a more positively charged $ZrCl_3$ surface. However, the absence of highly localized charge accumulation between $CO_2$ and surface atoms, together with the preservation of the molecular integrity of $CO_2$, suggests that the interaction is dominated by strong physisorption rather than true chemisorption. The adsorption is therefore driven primarily by electrostatic interactions and charge polarization effects, leading to a more positively charged $ZrCl_3$ surface without the formation of direct chemical bonds.

http://dx.doi.org/10.29356/jmcs.v70i1.2561

*J. Mex. Chem. Soc.* **2026**, *70(1):e2561*
Regular Issue

ISSN-e 2594-0317

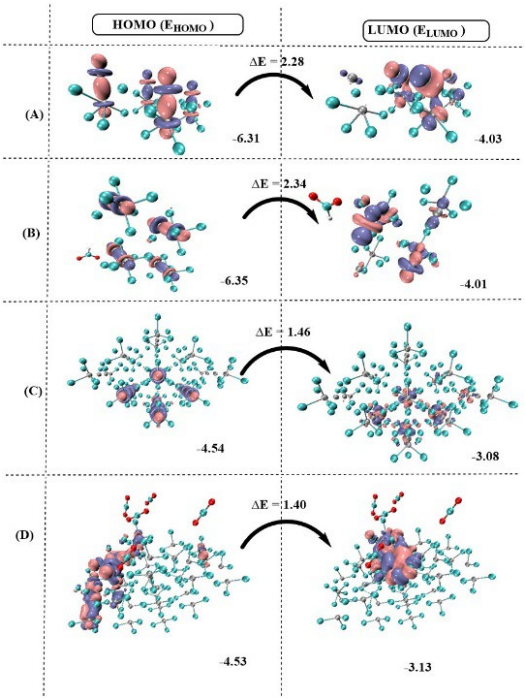


**Fig. 2.** Frontier molecular orbitals-transition state with the associated band energy computed for the optimized systems **(A)** $ZrCl_3$ unit cell, **(B)** $CO_2$ adsorption $ZrCl_3$ unit cell, **(C)** $ZrCl_3$ supercell, and **(D)** $CO_2$-multilayer $ZrCl_3$ supercell, with the PBE density functional approximation, (All energy values are computed with eV).

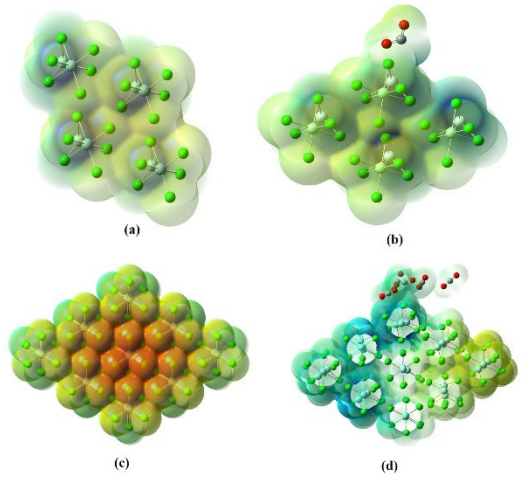


**Fig. 3.** Electrostatic potential map with color scale code (from more negative value to more positive value Orange→Yellow→Green→Blue) for **(a)** single $ZrCl_3$ cell, **(b)** $CO_2$ adsorption $ZrCl_3$ unit cell, **(c)** multilayer $ZrCl_3$ supercell, and **(d)** $CO_2$-multilayer $ZrCl_3$ supercell, with the PBE density functional approximation.

## Electronic band structure and density of states spectra of zirconium chloride crystal

As is well known, computationally generated electronic band structure (EBS) and density of states (DOS) spectra provide a vivid image of energetic states [48]. Fig. 4 displays the two types of studied spectra

*J. Mex. Chem. Soc.* **2026**, *70(1):e2561*
Regular Issue

ISSN-e 2594-0317

for $ZrCl_3$ crystal structure. The successive electronic levels present with calculated Fermi level at 0 K, represent several states contributed in the occupied and virtual areas with the specific *k*-points generated in a highly symmetric sample. Since DOS specifies the amount of energy states present at a given energy, it is a crucial metric in the field of solid-state physics for describing the mobility states of electrons [49]. Because Zr and Cl atoms with 1:3 ratio represent electron deficiency and electron-rich sites, respectively, it was expected that the electron excitation from the p orbital of Cl to the d orbital of Zr would be the majority in the partial DOS (PDOS) contribution. The findings confirm the presence of a highly contributed d orbital in the virtual and occupied levels (green lines). While more contribution of p orbital (red line) is exported from both Zr and Cl atoms. The band gap calculated for the overall solid-state crystal at the same level of optimization was 2.350 eV, that consistent with semiconducting systems.

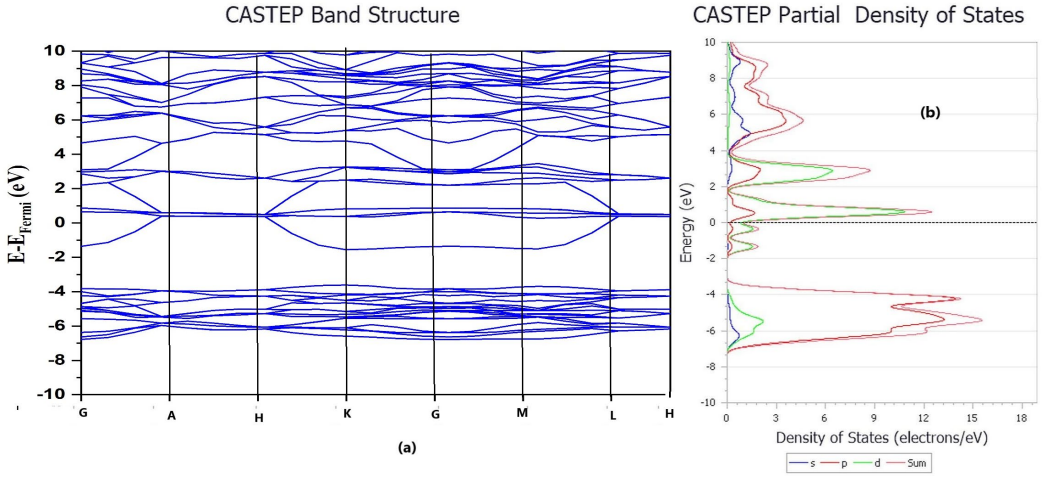


**Fig. 4.** EBS and DOS spectra of $ZrCl_3$ crystal structure with group space P63/MCM.

## Effect of adsorption on molecular dynamics simulation

Molecular Dynamics (MD) simulation represents an efficient computational technique to study the time-dependent motions of atoms and molecules. Deep insights into the mechanical, electrical, and structural properties of several modified systems based on atomic mobility properties during a simulation period **[50].** The dynamic simulation's temperature control examined how the separated and adsorbed systems behaved similarly as depicted in Figures 5-8. The studied systems involve a significant variation in flocculated temperature based on the system characteristic towards $CO_2$ adsorption molecules. $CO_2$-capacity on the surface of the $ZrCl_3$ system controls the dynamic movement and effect on stabilization through the time of simulation. As seen from Figures 5 and 6, the presence of 1-2 $CO_2$ molecules increases the average value of temperature from 350 K to 650 K. However, the pristine $ZrCl_3$ system (Fig.7) is dynamically affected at temperatures up to 450 K at a simulation time of 1500 ps with significant flocculation of atomic movement during the simulation time. At the end of the simulation (10000 ps), the two $CO_2$-loaded systems flocculate slightly with some stability towards 300 K as an average value. The simulation stability of the $CO_2$ adsorption systems gives a good indication of the favorable binding affinity on the surface of the crystal compared with the separate $ZrCl_3$ supercell as in Fig. 7. Fig. 8 presents a significant atomic dynamic movement during the simulation time; this predicts the high mobility of $CO_2$ molecules on the surface of $ZrCl_3$ supercell during simulation. The adsorbate arrangement on the surface before simulation specifically closed to Zr atoms with one oxygen atom as depicted in Fig. 8**(a)**. While at the end of simulation time (Fig. 8**(b)**), $CO_2$ molecules penetrated the surface to be in the bulk of the system with high flocculation at a maximum temperature of 380 K. The results concluded a more stable $CO_2$-unit cell adsorption system with a high capacity of adsorbate on the surface.

http://dx.doi.org/10.29356/jmcs.v70i1.2561

*J. Mex. Chem. Soc.* **2026**, *70(1):e2561*
Regular Issue

ISSN-e 2594-0317

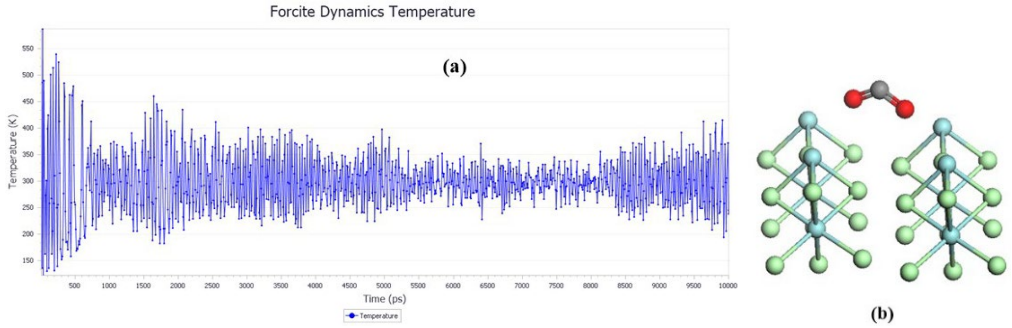


**Fig. 5.** Molecular dynamic simulation of temperature with time (a), of $ZrCl_3$ unit cell with one molecule of $CO_2$ **(b)**.

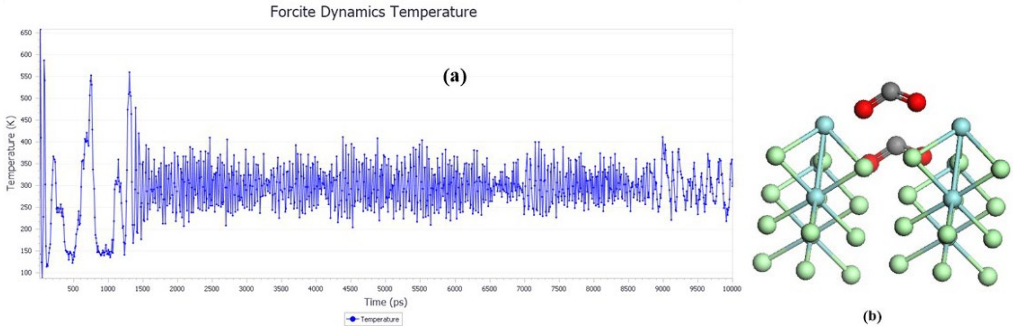


**Fig. 6.** Molecular dynamic simulation of temperature with time **(a)**, $ZrCl_3$ unit cell with two molecules of $CO_2$ **(b)**.

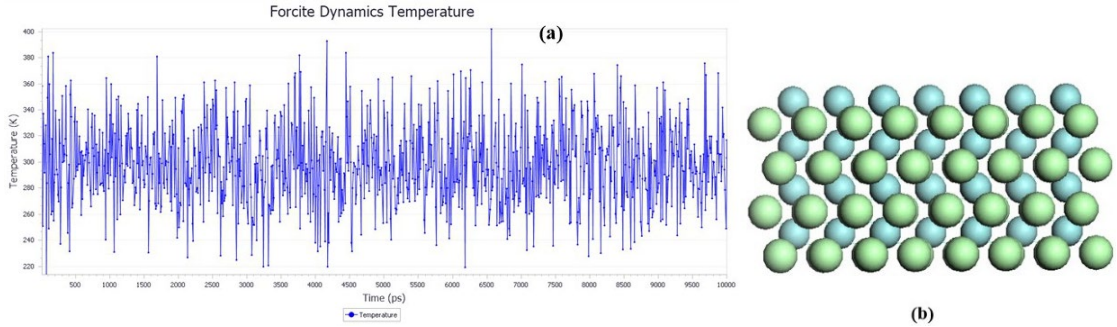


**Fig. 7.** Molecular dynamic simulation of temperature with time **(a)** of $ZrCl_3$ supercell **(b)**.

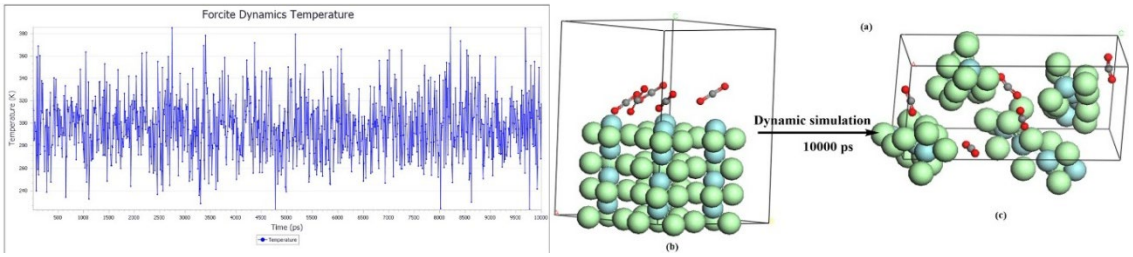


**Fig. 8.** Molecular dynamic simulation and temperature effect on $ZrCl_3$ supercell with 3 molecules of $CO_2$ **(a)**, the supercell system before simulation **(b)**, and the supercell system after simulation **(c)**.

http://dx.doi.org/10.29356/jmcs.v70i1.2561

*J. Mex. Chem. Soc.* **2026**, *70(1):e2561*
Regular Issue

ISSN-e 2594-0317

In molecular dynamics simulations, potential energy ($E_{pot}$) and kinetic energy ($E_{kin}$) serve as the primary energetic descriptors for assessing the stability and thermal state of a system; potential energy accounts for the internal forces between atoms, including bond stretching, van der Waals interactions, and electrostatic forces. While kinetic energy is directly proportional to the system's temperature and represents the motion of the particles. The provided study illustrates the thermodynamic stability of different $ZrCl_3$ configurations through MD simulations over a 10000 ps trajectory, where the achievement of steady-state fluctuations in these energies confirms system equilibration. In Fig. 9, representing a unit cell with one $CO_2$ molecule, the potential energy stabilizes with minimal kinetic energy noise, indicating a highly stable, low-resistance interaction. Fig. 10 shows that increasing the loading to two $CO_2$ molecules introduces significant initial kinetic oscillations and a longer equilibration period of roughly 1500 ps, suggesting a more complex structural reorganization phase as the molecules compete for optimal binding sites. Finally, Fig.11 transitions to a larger supercell containing three $CO_2$ molecules, resulting in a significantly higher potential energy baseline; this system exhibits broader kinetic fluctuations, which is characteristic of the increased degrees of freedom and the longer time-scales required for larger periodic structures to reach a global minimum. Collectively, these plots serve as a validation of the simulation parameters, proving that the $CO_2$ molecules have been successfully integrated into the $ZrCl_3$ framework without causing structural collapse.

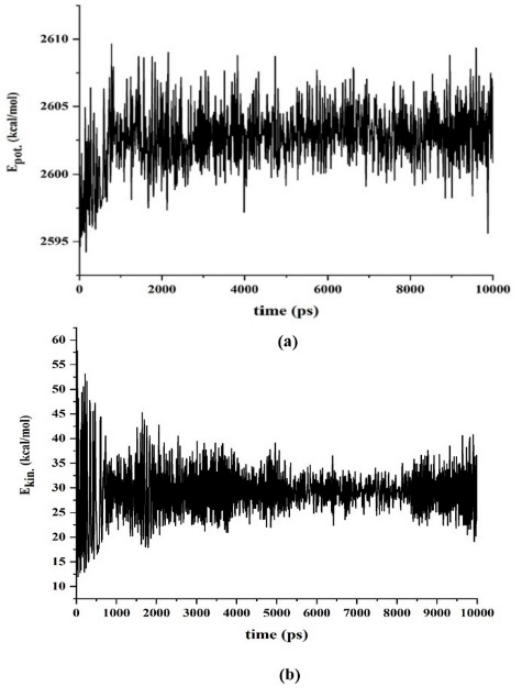


**Fig. 9. (a)** potential energy variable, **(b)** kinetic energy variable, of $ZrCl_3$ unit cell with one molecule of $CO_2$ $ZrCl_3$ unit cell with one molecule of $CO_2$.

http://dx.doi.org/10.29356/jmcs.v70i1.2561

*J. Mex. Chem. Soc.* **2026**, *70(1):e2561*
Regular Issue

ISSN-e 2594-0317

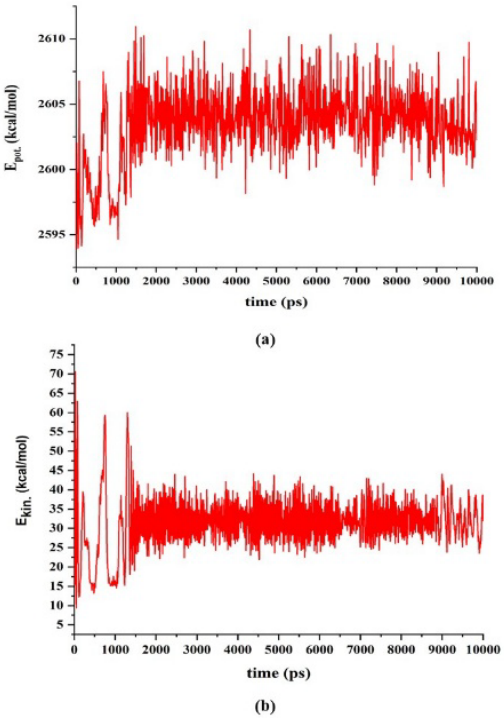


**Fig. 10. (a)** potential energy variable, **(b)** kinetic energy variable, of unit cell with two molecules of $CO_2$.

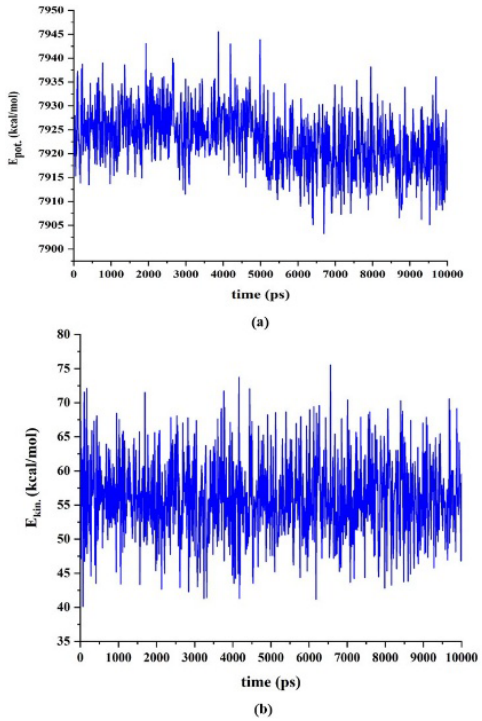


**Fig. 11. (a)** potential energy variable, **(b)** kinetic energy variable, of $ZrCl_3$ supercell with 3 molecules of $CO_2$.

http://dx.doi.org/10.29356/jmcs.v70i1.2561

*J. Mex. Chem. Soc.* **2026**, *70(1):e2561*
Regular Issue

ISSN-e 2594-0317

**Hydrated simulation systems using adsorption annealing**

Reducing greenhouse gas emissions from major sources and ambient air can be achieved using one of the most promising approaches: carbon capture [51]. $CO_2$ adsorption is one of the most used ways because it requires little energy. Water vapor may be found in almost all $CO_2$-rich industrial gas streams in the atmosphere, making it critical to understand how it influences $CO_2$ adsorption. Water has a wide range of functions due to the wide variety of adsorbents; it can be a strong inhibitor of $CO_2$ adsorption or a great stimulator. Water may also have the reverse effect or speed up the rate of $CO_2$ collection. In this part, the adsorption of $CO_2$ aggregations on the surface of $ZrCl_3$ system in the presence of water molecules can predict the interaction ability of $CO_2$ to the hydrated Zr-based system. Fig. 12 demonstrates the $ZrCl_3$ unit cell system loading 3 molecules of $CO_2$ and 20 molecules of $H_2O$. The six studied models estimated an effective adsorption energy value of -2.03 eV, -2.01 eV, -2.00 eV, -1.97 eV, and -1.96 eV, from model 1 to model 6, respectively. $CO_2$ molecules in these models mostly interacted with water molecules through H-bond formation with specific bond lengths based on the conformational structure of the system. Other close interactions are present between O of $CO_2$ and Zr and between $H_2O$ and Cl, leading to a hydrated $CO_2$-$ZrCl_3$ stable system. Fig. 13 displays the adsorption models on the $ZrCl_3$ supercell and similar results of stability were discovered with differences in the adsorption energy values of the models owing to the higher loading system. The adsorption energy of the supercell models ranges from -2.00 eV to -1.93 eV. Fig. 14 shows the $CO_2$-adsorption locator fields (green dots) for both unicell and supercell systems that loaded during simulation. It is concluded the presence of $CO_2$ molecules closer to the surface of $ZrCl_3$ in the unit cell system more than in the supercell system. This observation predicts as the material surface becomes higher in size; the adsorbate distributes itself freely inside the hydration layer to be the more interacted $H_2O$ molecules. While the unit cell and supercell models of $ZrCl_3$ share the same crystallographic framework, their relevance to $CO_2$ adsorption differs due to surface exposure, coordination environment, and electrostatic polarization effects. The selected surface orientation exposes Zr centers coordinated by chloride ligands, creating anisotropic charge distributions that act as preferential adsorption sites for the quadrupolar $CO_2$ molecule. These exposed Zr–Cl motifs generate localized electrostatic fields that govern the initial orientation and anchoring of $CO_2$, as corroborated by MEP and adsorption locator analyses.

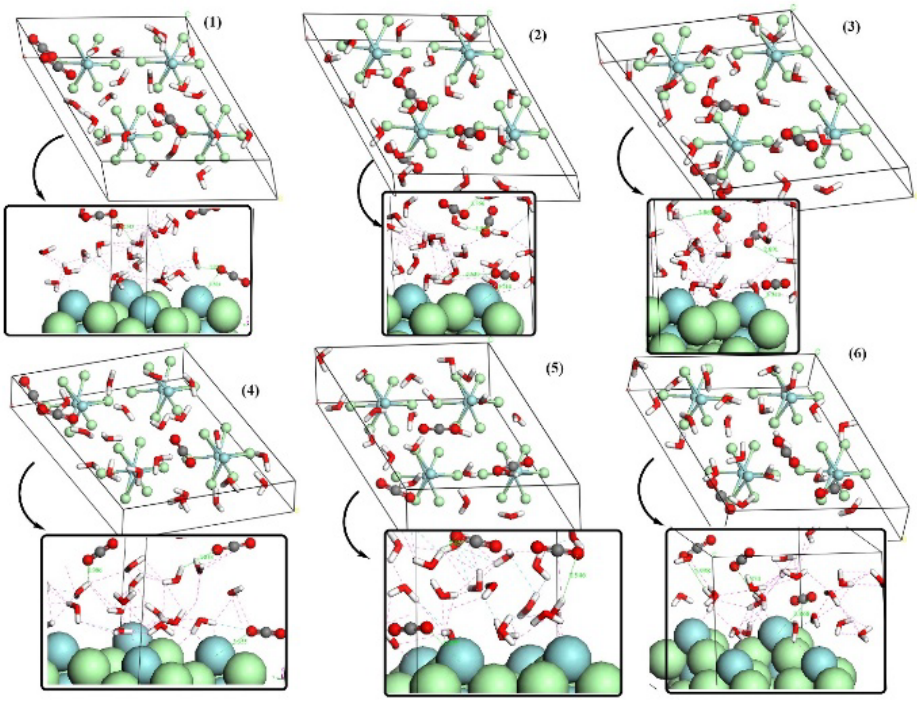


**Fig. 12.** $CO_2$-Hydrated $ZrCl_3$ unit cell adsorption annealing with several locator models.

http://dx.doi.org/10.29356/jmcs.v70i1.2561

*J. Mex. Chem. Soc.* **2026**, *70(1):e2561*
Regular Issue

ISSN-e 2594-0317

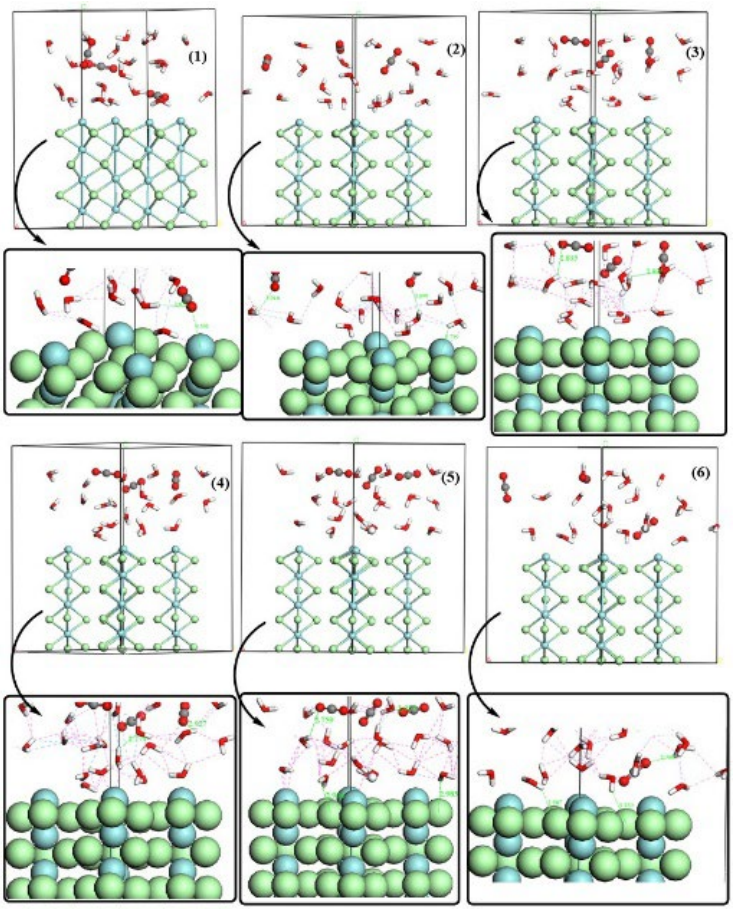


**Fig. 13.** $CO_2$-Hydrated $ZrCl_3$ supercell adsorption annealing with several locator models.

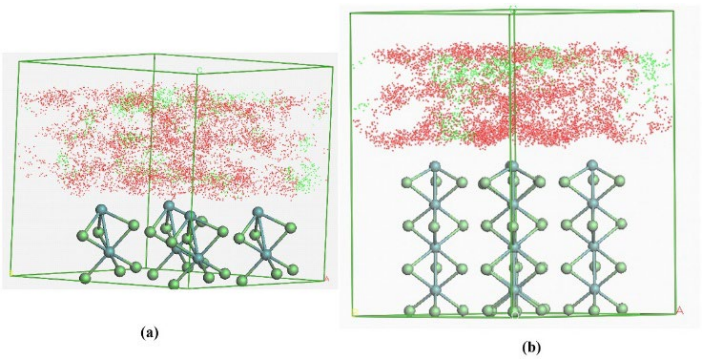


**Fig. 14.** Field locators of hydrated adsorption systems, **(a)** $CO_2$-hydrated $ZrCl_3$ unit cell, and **(b)** $CO_2$-hydrated $ZrCl_3$ supercell with red dots for water molecules and green dots of $CO_2$ molecules.

To support the findings of this work, previous research related to other system candidates was conducted. The zeolite of Si/Al ratio is low can possess a higher $CO_2$ adsorption capacity (2.8 mmol $g^{-1}$), with

http://dx.doi.org/10.29356/jmcs.v70i1.2561

*J. Mex. Chem. Soc.* **2026**, *70(1):e2561*
Regular Issue

ISSN-e 2594-0317

a much higher enthalpy of adsorption [52]. The adsorption capacity of $CO_2$ (MIL-53) (agZIF-62) CGC was found to be around 2.5 mmol/g, indicating its efficacy in preserving the properties of doped MOF crystals [53,54]. It was discovered that the addition of $ZrO_2$ could greatly improve the methanol selectivity of the InCo catalyst. Furthermore, increased oxygen vacancy and strong interaction between the In-Co-Zr catalysts contribute to improved $CO_2$ adsorption strength and capacity [55]. The structural, and electrical origins of molecule adsorption are investigated using experimental and DFT computations [56]. Experimental and computational results indicate that $CO_2$ adsorption on amorphous $ZrO_2$ (am-$ZrO_2$) surfaces is less uniform and generally weaker compared to crystalline zirconia. Since the electronic charge distribution and band structure of crystalline and amorphous $ZrO_2$ are largely similar, the reduced adsorption strength on am-$ZrO_2$ is attributed to the presence of fewer but stronger Zr–O surface bonds. These results offer detailed molecular-level understanding of $CO_2$ and general molecular adsorption behavior on $ZrO_2$-based catalytic materials.

This study summarized the mechanistic perspective, $CO_2$ adsorption on hydrated $ZrCl_3$ which proceeds through a cooperative, water-mediated electrostatic stabilization mechanism rather than direct chemisorption. The initial adsorption step is governed by the strong polarization of the $ZrCl_3$ surface, which induces electrostatic attraction between the partially positive carbon atom of $CO_2$ and electron-rich surface regions, while water molecules act as structural and electronic mediators. The formation of an extended hydrogen-bonding network between $CO_2$ and $H_2O$ stabilizes the adsorbate within the hydration layer, simultaneously facilitating secondary interactions between $CO_2$ oxygen atoms and Zr centers, as well as between water hydrogen atoms and surface Cl sites. This synergistic interaction network lowers the overall adsorption energy to approximately −2.0 eV, indicating a thermodynamically favorable yet structurally non-destructive adsorption process. As the system size increases from unit cell to supercell, the enhanced configurational freedom allows $CO_2$ molecules to redistribute within the hydration layer, reducing direct surface confinement while preserving adsorption stability. This behavior confirms that $CO_2$ capture on $ZrCl_3$ is driven by a balance between surface electrostatic fields, hydrogen-bond-assisted stabilization, and lattice flexibility, providing a realistic representation of adsorption under humid, industrially relevant conditions.

## Comparative assessment of $CO_2$ adsorption mechanisms in related materials

A direct quantitative comparison between $ZrCl_3$ and established $CO_2$ adsorbents such as zeolites, metal–organic frameworks (MOFs), and $ZrO_2$-based materials must be approached cautiously due to fundamental differences in structure, surface chemistry, and adsorption mechanisms. Zeolites with low Si/Al ratios typically exhibit high $CO_2$ uptake driven by strong electrostatic interactions between $CO_2$ quadrupoles and framework cations, resulting in high adsorption enthalpies but often accompanied by pronounced sensitivity to water vapor, which can competitively block active sites [57]. In contrast, many MOFs, including MIL-53 and ZIF-based composites, rely on well-defined pore architectures and coordinatively unsaturated metal sites to achieve high adsorption capacities (~2.5 mmol $g^{-1}$), yet their performance may degrade under humid conditions due to framework flexibility or water-induced pore occupation [58,59].

$ZrO_2$-based materials provide a more structurally relevant comparison to $ZrCl_3$ due to the presence of zirconium-centered adsorption sites. In crystalline $ZrO_2$, $CO_2$ adsorption is enhanced by surface oxygen vacancies and strong Zr–O interactions, which promote chemisorptive binding and higher adsorption strength [60]. However, experimental and DFT studies have shown that amorphous $ZrO_2$ exhibits weaker and less uniform $CO_2$ adsorption despite similar electronic band structures, primarily due to the reduced availability and accessibility of reactive Zr sites [61]. Compared to these systems, $ZrCl_3$ displays a distinct adsorption mechanism characterized by moderate adsorption energies (~−2.0 eV), surface polarization, and water-mediated stabilization rather than vacancy-driven chemisorption. This places $ZrCl_3$ in an intermediate regime between strong chemisorption (e.g., defective $ZrO_2$) and weak physisorption (e.g., purely porous frameworks), offering a favorable balance between adsorption strength, reversibility, and hydration tolerance.

Overall, while $ZrCl_3$ does not directly compete with high-capacity porous adsorbents in terms of gravimetric uptake, its adsorption behavior under hydrated conditions highlights a complementary capture strategy based on electronic adaptability and surface-mediated stabilization. This comparison underscores the relevance of $ZrCl_3$ as a structurally resilient, humidity-tolerant $CO_2$ adsorbent rather than a direct substitute for conventional zeolites or MOFs.

http://dx.doi.org/10.29356/jmcs.v70i1.2561

*J. Mex. Chem. Soc.* **2026**, *70(1):e2561*
Regular Issue

ISSN-e 2594-0317

## Conclusions

This study elucidates the dual structural and electronic response of $ZrCl_3$ to $CO_2$ adsorption, highlighting the importance of model dimensionality in capturing realistic surface phenomena. Our findings transition from a localized molecular perspective to a periodic crystalline framework, revealing that $CO_2$ sequestration is governed by a significant electronic reconfiguration. The observed reduction in the energy gap to 1.40 eV upon adsorption suggests that $CO_2$ introduces mid-gap states, effectively narrowing the forbidden zone and potentially enhancing the material's photo-responsiveness or surface conductivity. The observed differences in adsorption energy, $CO_2$ distribution, and electronic structure between unit cell and supercell models demonstrate that increasing surface dimensionality enhances the physical realism of the adsorption process. Specifically, the supercell better represents extended surface polarization and adsorbate mobility within the hydration layer, while preserving the local Zr-centered binding motif identified in the unit cell. Thus, the combined use of unit cell and supercell models enables a hierarchical interpretation of $CO_2$ adsorption, linking local coordination chemistry to collective surface behavior. The electronic structure analysis confirms that bulk $ZrCl_3$ is a wide-bandgap semiconductor ($E_g \approx 2.35$ eV), indicating limited intrinsic electrical conductivity under ambient conditions. Consequently, the adsorption behavior observed in this study is governed by surface electrostatics and local electronic redistribution rather than charge transport or metallic conduction.The electrostatic potential analysis demonstrates that the supercell model provides a more realistic representation of the extended surface environment, capturing long-range Coulombic effects and enhanced surface potential heterogeneity that are not accessible within a primitive unit cell description. These features play a decisive role in stabilizing $CO_2$ near Zr-centered adsorption sites. Molecular dynamics simulations further reveal that adsorption stability arises from structural flexibility rather than rigid lattice confinement. While the unit cell exhibits constrained geometrical relaxation, the supercell allows subtle lattice adjustments that accommodate $CO_2$ without disrupting the crystal framework, highlighting the importance of configurational freedom in realistic surface–adsorbate interactions. Importantly, the inclusion of an explicit hydration layer shows that $CO_2$ adsorption remains energetically favorable even under aqueous conditions, where stabilization is achieved through a cooperative interplay of water-mediated hydrogen bonding and electrostatic attraction to surface Zr centers.

Overall, this study demonstrates that $ZrCl_3$ can act as a structurally resilient $CO_2$ capture material, with adsorption driven by surface electrostatics and lattice adaptability rather than electronic conductivity. These insights underscore the necessity of combining supercell models, band-structure-based electronic analysis, and dynamical simulations to achieve a physically consistent description of adsorption processes on semiconducting surfaces.

## References

1. Mitchell, S.; Qin, R.; Zheng, N.; et al. *Nat. Nanotechnol.* **2021**, *16*, 129–139. DOI: https://doi.org/10.1038/s41565-020-00799-8
2. Lanzafame, P.; Perathoner, S.; Centi, G.; Gross, S.; Hensen, E. J. M. *Catal. Sci. Technol.* **2017**, *7*, 5182–5194.
3. Mitchell, S.; Martín, A. J.; Pérez-Ramírez, J. *Nat. Chem. Eng.* **2024**, *1*, 13–15. DOI: https://doi.org/10.1038/s44286-023-00005-1
4. Naveen, K. E.; Raju, K.; Beenarani, B. B.; Alsharif, M. H.; Kim, M. K.; Hasan, Z. I. *Energy Rep.* **2024**, *11*, 1171–1190. DOI: https://doi.org/10.1016/j.egyr.2023.12.068
5. Shen, Z.; Han, Q.; Luo, X.; et al. *Nat. Photonics.* **2024**, *18*, 450–457. DOI: https://doi.org/10.1038/s41566-024-01383-5
6. Li, S.; Jiang, Y.; Xu, J.; et al. *Nature.* **2024**. DOI: https://doi.org/10.1038/s41586-024-08103-7
7. *Nat. Energy.* **2019**, *4*, 1. DOI: https://doi.org/10.1038/s41560-018-0323-9
8. Hamad, A.; Jia, B. *Int. J. Environ. Res. Public Health.* **2022**, *19*, 11278. DOI: https://doi.org/10.3390/ijerph191811278

*J. Mex. Chem. Soc.* **2026**, *70(1):e2561*
Regular Issue

ISSN-e 2594-0317


9. El, S.; Abdelrehim, E. M. *Spectrochim. Acta Part A Mol. Biomol. Spectrosc.* **2021**, *261*, 120006. DOI: https://doi.org/10.1016/j.saa.2021.120006
10. Ibraheem, H. H.; Ali, A. I.; El-Sayed, D. S. *J. Mol. Struct.* **2024**, 138484. DOI: https://doi.org/10.1016/j.molstruc.2024.138484
11. Issa, A. A.; Ibraheem, H. H.; El-Sayed, D. S. *J. Mol. Model.* **2024**, *30*, 14. DOI: https://doi.org/10.1007/s00894-023-05815-x
12. Zhang, Y.; Kitchaev, D. A.; Yang, J.; et al. *npj Comput. Mater.* **2018**, *4*, 9. DOI: https://doi.org/10.1038/s41524-018-0065-z
13. Marzari, N.; Ferretti, A.; Wolverton, C. *Nat. Mater.* **2021**, *20*, 736–749. DOI: https://doi.org/10.1038/s41563-021-01013-3
14. Wu, L.; Zhu, Y.; Yuan, J.; Guo, X.; Zhang, Q. *Energies.* **2024**, *17*, 1861. DOI: https://doi.org/10.3390/en17081861
15. Sarikas, A. P.; Gkagkas, K.; Froudakis, G. E. *Sci. Rep.* **2024**, *14*, 27360. DOI: https://doi.org/10.1038/s41598-024-76319-8
16. Broom, D. P. *Adsorption.* **2024**, *30*, 1565–1591. DOI: https://doi.org/10.1007/s10450-023-00424-9
17. Yuan, Y.; Wang, J.; Adimi, S.; et al. *Nat. Mater.* **2020**, *19*, 282–286. DOI: https://doi.org/10.1038/s41563-019-0535-9
18. Kazanskiy, N. L.; Butt, M. A.; Khonina, S. N. *Nanomaterials.* **2022**, *12*, 2171. DOI: https://doi.org/10.3390/nano12132171
19. Iqbal, M. A.; Malik, M.; Anwar, N.; et al. *Arab. J. Chem.* **2023**, *16*, 105040. DOI: https://doi.org/10.1016/j.arabjc.2023.105040
20. Zhang, F.; Zhou, Y.; Chen, Z.; et al. *Adv. Mater.* **2022**, *34*, 2204801. DOI: https://doi.org/10.1002/adma.202204801
21. Shyam, L. G.; Kumar, S.; et al. *Int. J. Hydrogen Energy.* **2023**, *55*, 1465–1475. DOI: https://doi.org/10.1016/j.ijhydene.2023.11.286
22. Faizan, M.; Bhamu, K. C.; Murtaza, G.; et al. *Sci. Rep.* **2021**, *11*, 6965. DOI: https://doi.org/10.1038/s41598-021-86145-x
23. Curtarolo, S.; Hart, G.; Nardelli, M.; et al. *Nat. Mater.* **2013**, *12*, 191–201. DOI: https://doi.org/10.1038/nmat3568
24. Louie, S. G.; Chan, Y. H.; da Jornada, F. H.; et al. *Nat. Mater.* **2021**, *20*, 728–735. DOI: https://doi.org/10.1038/s41563-021-01015-1
25. Lu, Z. *Mater. Rep. Energy.* **2021**, *1*, 100047. DOI: https://doi.org/10.1016/j.matre.2021.100047
26. Jain, A.; Shin, Y.; Persson, K. *Nat. Rev. Mater.* **2016**, *1*, 15004. DOI: https://doi.org/10.1038/natrevmats.2015.4
27. Wu, X.; Kang, F.; Duan, W.; Li, J. *Prog. Nat. Sci. Mater. Int.* **2019**, *29*, 247–255. DOI: https://doi.org/10.1016/j.pnsc.2019.04.003
28. Sepehri, A.; Loeffler, T. D.; Chen, B. *J. Chem. Phys.* **2014**, *141*. DOI: https://doi.org/10.1063/1.4892640
29. http://accelrys.com/products/collaborative-science/biovia-materials-studio/, accessed in December 2022.
30. Vásquez, G. C.; Maestre, D.; Cremades, A.; et al. *Sci. Rep.* **2018**, *8*, 8740. DOI: https://doi.org/10.1038/s41598-018-26728-3
31. Issa, A. A.; Kamel, M. D.; El-Sayed, D. S. *J. Mol. Model.* **2024**, *30*, 106. DOI: https://doi.org/10.1007/s00894-024-05896-2
32. Clark, S. J.; Segall, M. D.; Pickard, C. J.; Hasnip, P. J.; Probert, M. I.; Refson, K.; Payne, M. C. *Z. Kristallogr.* **2005**, *220*, 567–570. DOI: https://doi.org/10.1524/zkri.220.5.567.65075
33. Choudhary, K.; Zhang, Q.; Reid, A.; et al. *Sci. Data.* **2018**, *5*, 180082. DOI: https://doi.org/10.1038/sdata.2018.82
34. Mahmood, W. K.; Dakhal, G. Y.; Younus, D.; et al. *J. Mol. Model.* **2024**, *30*, 165. DOI: https://doi.org/10.1007/s00894-024-05956-7

ISSN-e 2594-0317

35. Jafarova, V. N.; Orudzhev, G. S. *Solid State Commun.* **2021**, *325*, 114166. DOI: https://doi.org/10.1016/j.ssc.2020.114166
36. El-Sayed, D. S. *J. Mol. Model.* **2023**, *29*, 96. DOI: https://doi.org/10.1007/s00894-023-05501-y
37. Fiedler, L.; Modine, N. A.; Schmerler, S.; et al. *npj Comput. Mater.* **2023**, *9*, 115. DOI: https://doi.org/10.1038/s41524-023-01070-z
38. Pedone, A.; Presti, D.; Menziani, M. C. *Chem. Phys. Lett.* **2012**, *541*, 12–15. DOI: https://doi.org/10.1016/j.cplett.2012.05.049
39. Sun, S. Y.; Nie, X. Y.; Huang, J.; Yu, J. G. *J. Membr. Sci.* **2019**, *595*, 117528. DOI: https://doi.org/10.1016/j.memsci.2019.117528
40. Gao, W.; Chen, Y.; Li, B.; Liu, S. P.; Liu, X.; Jiang, Q. *Nat. Commun.* **2020**, *11*, 1196. DOI: https://doi.org/10.1038/s41467-020-14969-8
41. Brauer, B.; Kesharwani, M. K.; Martin, J. M. L. *J. Chem. Theory Comput.* **2014**, *10*, 3791–3799. DOI: https://doi.org/10.1021/ct500513b
42. Shuttleworth, I. G. *J. Phys. Chem. Solids.* **2015**, *86*, 19–26. DOI: https://doi.org/10.1016/j.jpcs.2015.06.016
43. Elessawy, N. A.; Exley, J.; El-Sayed, D. S.; et al. *J. Environ. Chem. Eng.* **2024**, 112489. DOI: https://doi.org/10.1016/j.jece.2024.112489
44. Mahmoud, M. E.; Salma, T. H.; Khalil, T. E.; et al. *J. Mol. Liq.* **2023**, *390*, 123042. DOI: https://doi.org/10.1016/j.molliq.2023.123042
45. Fukui, K.; Yonezawa, T.; Shingu, H. *J. Chem. Phys.* **1952**, *20*, 722–725. DOI: https://doi.org/10.1063/1.1700523
46. Bayly, C. I.; Cieplak, P.; Cornell, W.; Kollman, P. A. *J. Phys. Chem.* **1993**, *97*, 10269–10280. DOI: https://doi.org/10.1021/j100142a004
47. Knøsgaard, N. R.; Thygesen, K. S. *Nat. Commun.* **2022**, *13*, 468. DOI: https://doi.org/10.1038/s41467-022-28122-0
48. DeMille, D.; Hutzler, N. R.; Rey, A. M.; et al. *Nat. Phys.* **2024**, *20*, 741–749. DOI: https://doi.org/10.1038/s41567-024-02499-9
49. Maskery, I.; Sturm, L.; Aremu, A. O.; et al. *Polymer.* **2018**, *152*, 62–71. DOI: https://doi.org/10.1016/j.polymer.2017.11.049
50. Li, S.; Chen, R.; Wang, J.; et al. *npj Mater. Sustain.* **2024**, *2*, 11. DOI: https://doi.org/10.1038/s44296-024-00014-y
51. Boer, D. G.; Langerak, J.; Pescarmona, P. P. *ACS Appl. Energy Mater.* **2023**, *6*, 2634–2656. DOI: https://doi.org/10.1021/acsaem.2c03605
52. Li, N.; Ma, C.; Wang, Z.; Li, D.; Qiao, Z.; Zhong, C. *J. Membr. Sci.* **2024**, 123453. DOI: https://doi.org/10.1016/j.memsci.2024.123453
53. Ashling, C. W.; Johnstone, R. N.; Widmer, J. W.; et al. *J. Am. Chem. Soc.* **2019**, *141*, 15641–15648.
54. Nuermaimaitijiang, W.; Shen, R.; Hao, L.; et al. *Chem. Eng. J.* **2024**, *501*, 157397. DOI: https://doi.org/10.1016/j.cej.2024.157397
55. Joutsuka, T.; Tada, S. *J. Phys. Chem. C.* **2023**, *127*, 6998–7008. DOI: https://doi.org/10.1021/acs.jpcc.3c01185
56. Cavenati, S.; Grande, C. A.; Rodrigues, A. E. *J. Chem. Eng. Data.* **2004**, *49*, 1095–1101. DOI: https://doi.org/10.1021/je0498917
57. Millward, A. R.; Yaghi, O. M. *J. Am. Chem. Soc.* **2005**, *127*, 17998–17999. DOI: https://doi.org/10.1021/ja0570032
58. Banerjee, R.; Phan, A.; Wang, B.; et al. *Science.* **2008**, *319*, 939–943. DOI: https://doi.org/10.1126/science.1152516
59. Zheng, H.; Jiang, Z.; Zhai, H.; Zheng, Z.; Wang, P.; Wang, Z.; Liu, Y.; Qin, X.; Zhang, X.; Huang, *Appl. Catal. B: Environ.* **2019**, *243*, 381–385. https://doi.org/10.1016/j.apcatb.2018.10.053
60. Siahrostami, S.; Tripkovic, V.; Rossmeisl, J.; Nørskov, J. K. *J. Phys. Chem. C.* **2016**, *120*, 24164–24172. DOI: https://doi.org/10.1021/acs.jpcc.6b07145